International Journal of Mass Spectrometry 280 (2009) 72–77

Contents lists available at ScienceDirect

International Journal of Mass Spectrometry

journal homepage: www.elsevier.com/locate/ijms

Velocity selection and mass spectrometric detection of an H_2S molecular beam and a collisional study of its interactions with rare gases

Vincenzo Aquilanti [a,*], David Cappelletti [b], Fernando Pirani [a], Luiz F. Roncaratti [a]

[a] Dipartimento di Chimica, Universitá di Perugia, 06123 Perugia, Italy
[b] Dipartimento di Ingegneria Civile ed Ambientale, Universitá di Perugia, 06125 Perugia, Italy

ARTICLE INFO

Article history:
Received 26 May 2008
Received in revised form 16 July 2008
Accepted 23 July 2008
Available online 3 August 2008

Keywords:
Molecular beam
Noncovalent interaction
Hydrogen bond

ABSTRACT

Total integral cross section experiments, for collisions of rotationally hot H_2S projectile molecules by He and Xe targets, have been performed in the thermal energy range by using a molecular beam apparatus, which operates under high resolution conditions and exploits a quadrupole mass spectrometer as a detector. Information on the radial dependence of the intermolecular interaction, averaged over all relative orientations of colliding partners, is obtained. This study completes the investigation of H_2S–rare gas family [see D. Cappelletti, A.F.A. Vilela, P.R.P. Barreto, R. Gargano, F. Pirani, V. Aquilanti, J. Chem. Phys. 125 (2006) 133111, for Ne, Ar and Kr] and permits us to discover similarities and differences with the analogous H_2O–Rg series of systems. In particular, the analysis of the scattering data suggests that while the complexes of H_2S–rare gases from He to Kr are essentially bound by nearly isotropic noncovalent interactions of van der Waals type, the H_2S–Xe system exhibits a weak, but measurable, additional component which emerges at intermediate intermolecular distance (in proximity of the potential well), and provides a bond stabilization. This observation is of possible interest for the investigation of the phenomenology of the hydrogen bond formation.

1. Introduction

The systematic experimental and theoretical investigation of homologous series of weakly bound molecular aggregates is a possible research strategy to cast light on the phenomenology of intermolecular forces and on their dependence on basic physical properties of the interacting partners. The present study is focused on the characterization, by high resolution molecular beam scattering experiments, of the leading interaction components of the H_2S–He and H_2S–Xe complexes, which are expected to be bound by weak noncovalent interactions. These experiments complete the series of total (elastic + inelastic) integral cross sections measurements on H_2S–Rg (Rg = rare gas atom) systems recently initiated in our laboratory [1]. Extensive *ab initio* calculations [1] were also carried out in parallel with the experiments, in order to characterize minima in the potential energy surfaces and energy barriers associated as a function of the relative orientation of the Rg atom with respect to the H_2S molecule.

Particular interest for H_2S–Rg systems arises from a recent experimental evidence that in the analogous H_2O–Rg aggregates [2,3] an additional contribution to the ubiquitous van der Waals (V_{vdW}) interaction was found. Herein, V_{vdW} is defined [2] as arising from the combination of size repulsion and dispersion attraction effects, accounting also for small induction contributions. The experiments on water complexes have shown that the additional component of the interaction emerges at intermediate and short distances and plays a role of increasing importance in the series going from He to Xe [2,3]. We correlated these experimental findings with the formation of an embryonic hydrogen bond structure. The question tackled here is to clarify whether also the H_2S–Rg aggregates exhibit a behavior similar to the analogous water complexes.

Section 2 provides a brief description of the experimental technique used to measure integral cross sections by molecular beam scattering and gives basic details of the calibration procedure of a new device, build up to perform the molecular beam velocity selection. Section 3 reports the data analysis, their discussion and some conclusions.

2. Experimental

2.1. Cross section measurements

The experimental apparatus used to perform the scattering experiments described in this paper consists of a set of differentially

* Corresponding author.
E-mail addresses: vincenzoaquilanti@yahoo.it (V. Aquilanti), david.cappelletti@unipg.it (D. Cappelletti).

1387-3806/$ – see front matter © 2008 Elsevier B.V. All rights reserved.
doi:10.1016/j.ijms.2008.07.026

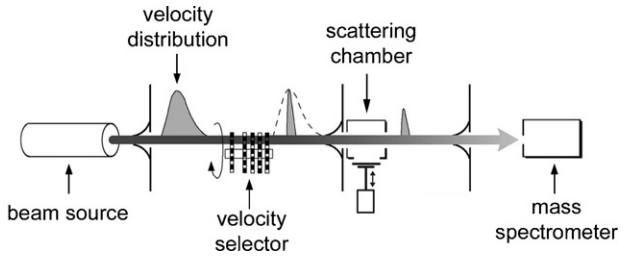

Fig. 1. Sketch of the experimental apparatus used to measure the integral cross section $Q(v)$ as a function of the selected beam velocity v.

pumped vacuum chambers connected by slits for the molecular beam collimation (see, e.g., [4] and references therein). The beam emerges through a nozzle (1 mm in diameter), from a source which can operate under effusive or moderately supersonic conditions. After mechanical velocity selection, the beam crosses a scattering chamber, which can be filled up with the target gas by an automated procedure. The on-line beam intensity is detected, after the scattering region, by an electron bombardment ionizer followed by a quadrupole mass spectrometer. A sketch of the apparatus is shown in Fig. 1, while details on slit dimensions and scattering chamber characteristics are given elsewhere [4]. The molecular beams have been generated by near effusive expansions of H_2S vapor through a nozzle heated to 500 K, in order both to suppress cluster formation and to "heat up" the rotational motion of the H_2S molecules. The signal detection in the mass spectrometer is made at $m/e = 34$ for which the best signal to noise ratio is achieved. H_2S has been kept in the source both pure, at a stagnation pressure of 5 mbar, and in a mixture with He at a total stagnation pressure ≤ 25 mbar, thus making it possible to cover a wide collision range. The molecular beam velocity analysis and selection have been obtained with the use of a new slotted disk velocity selector, described below. The measurement of the molecular beam attenuation I/I_0 (where I and I_0 represent the molecular beam intensity with and without target gas in the scattering chamber) at a selected velocity v, permits the determination of the total integral cross section $Q(v)$ as a function of the velocity v,

$$Q(v) = \frac{1}{NL} \log \frac{I_0}{I}, \tag{1}$$

where N is the target gas density and L is the length of the effective molecular beam path in the scattering chamber. The NL factor is empirically adjusted for each system varying the pressure of the target gas in the chamber, such as to have an I_0/I ratio ranging from 2 to 4 which allows minimization of the error associated with the beam intensity fluctuations and ion counting. The scattering chamber has been kept at liquid air temperature (~ 90 K), in order to enhance the velocity resolution of the experiments [4]. As previously, the absolute values of $Q(v)$ have been obtained by an internal calibration based on the direct measurement of the gas flow in the scattering chamber and on the absolute values of the He–Ar cross sections [5,6].

2.2. The velocity selector

As anticipated, the velocity selector is a newly built device, based on a design that we recently proposed [7] for surface scattering experiment. In the present case, the model has been modified with respect to the original one by increasing its length and adding more rotating disks, in order to improve the resolution power of the device. The present version is 194 mm long and made up of six rotating slotted disks. Each disk has been machined, from an aluminum sheet 0.20-mm thick, to a diameter of 150 mm. A sketch of a disk is reported in Fig. 2: 600 rectangular slits, 0.25 mm $\times$ 4.76 mm, have been indented in the border of each disk (indicated by a light shaded area in the figure) by a laser cutting technique. The slits are spaced out by a 0.50 mm wall (see the blow up in the upper part of the figure). At variance with the two-disk model of ref. [7], in the present six-disk case the spacing among the disks and the alignment of the slits are crucial features to define resolution and transmission power of the selector. As a consequence, the mounting of the disks on the rotating motor shaft of the selector has been particularly delicate. A design of the selector is reported in Fig. 3 (the molecular beam travels from left to right). The disks have been aligned in three pairs according to the sequence 1-2-3-2-3-1, as indicated in Fig. 3, varying the position of one reference slit with respect to a reference axis: the alignment angle ϕ is shown in Fig. 2. The disks labeled by 1 in Fig. 3 have an angular phase shift $\phi = 0.40^\circ$ (corresponding to 0.50 mm on the circumference of the disk); the disks labeled by 2 have an angular phase shift $\phi = 0.60^\circ$ (0.75 mm) and for the disks $3\phi = 0.20^\circ$ (0.25 mm).

A water cooled brushless dc servomotor (201 W) has been employed to drive the velocity selector. The motor rotation frequency f can be varied in the range 3–130 Hz, and is stabilized down to ± 0.05 Hz, by a feedback signal from an encoder (E in Fig. 3), mounted on the first external disk. As will be shown below, this mounting configuration allows the selection of molecules with a velocity v in the range 50–2200 m s^{-1} and with a FWHM (full width at half maximum) lower than 5%.

The performances of the mechanical velocity selector have been tested by producing a supersonic Ar beam emerging from a nozzle source hole (0.10 mm diameter) kept at room temperature and at a stagnation pressure of ~ 250 mbar. The transmitted beam intensity as a function of the rotational frequency of the slotted disks has been recorded in a wide range of frequencies. Results are reported in Fig. 4. Here the principal peak corresponds to the opening of

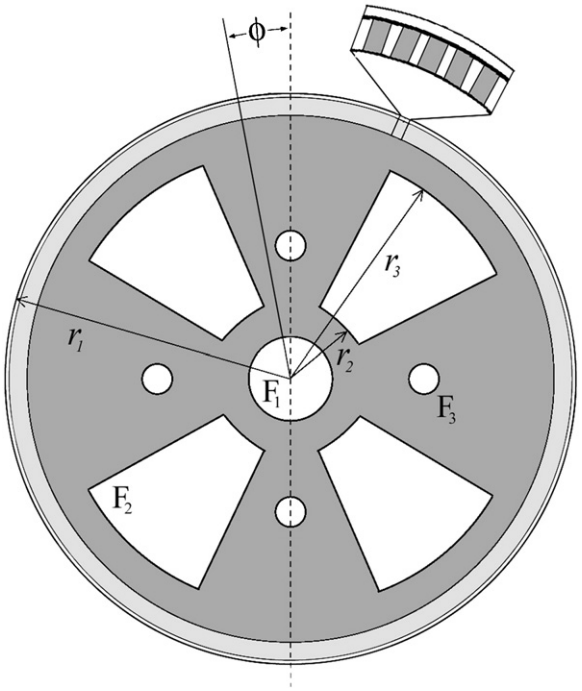

Fig. 2. Sketch of a disk of the velocity selector. The slits are cut in the external area of the disk (see the blow up). The distance from the center of the disk to the middle of the slits is 71.62 mm. The motor shaft passes through F_1. The F_2 areas have been carved out to lighten the disk which has a moment of inertia of ~ 200 g cm^2. Indicated distances from the center are: $r_1 = 75$ mm, $r_2 = 20$ mm, $r_3 = 61$ mm. The F_3 holes serve to insert the aligning bars.

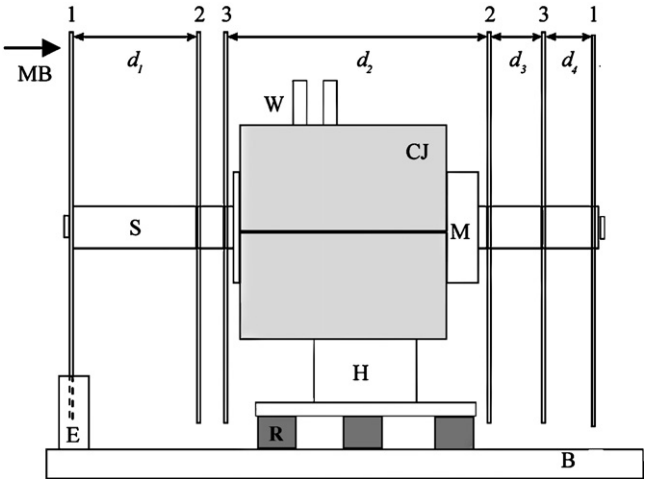

Fig. 3. Sketch of the mechanical velocity selector. The molecular beam (MB) travels from left to right; (W) water inlet/oulet; (CJ) copper cooling jackets; (H) aluminum holder; (R) rubber spacers; (M) motor; (S) motor shaft; (E) encoder, (B) movable stainless steel base. Distances are: $d_1 = 49.2$ mm; $d_2 = 13.1$ mm; $d_3 = 94.7$ mm; $d_4 = d_5 = 18.5$ mm.

the main helical path through the set of the rotating slotted disks. For the present mounting set-up, the main helical path is the one of order 7 (see ref. [7] for more details). The two lowest peaks at higher frequencies are due to residual sidebands, associated to the helical paths of order 11 and 21 (often called "undesired harmonics"). The full elimination of such sidebands would require the use of additional disks. However, these contributions are at most of the order 2–3% of the main peak and are also completely resolved for the case of supersonic molecular beams because of the sharp velocity distributions, as in the case described in Fig. 4. For nearly effusive molecular beams, the velocity distributions of the sidebands may overlap with the main one: it has been estimated that under the most unfavorable conditions the maximum effect on a measured integral cross section is of the order of about 1% (values comparable with the global uncertainty).

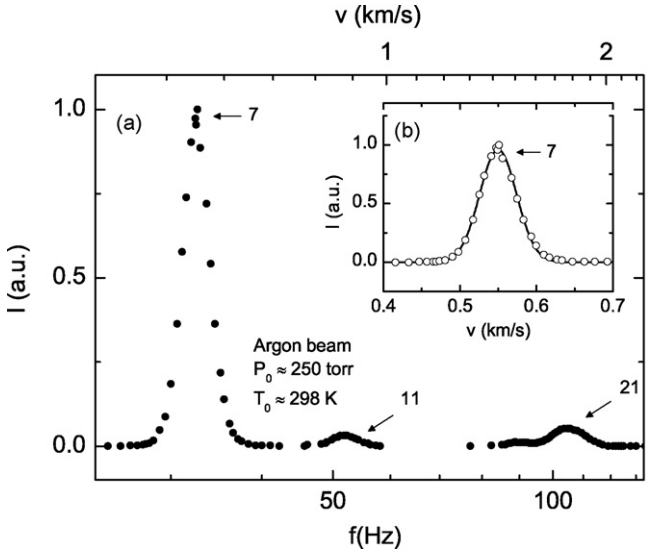

Fig. 4. Transmitted Ar beam intensity I measured as a function of the rotational frequency f of the mechanical velocity selector. The inset compares measured data (circles) with calculation (full line) corresponding to a velocity distribution function evaluated at source temperature of 298 K and Mach number of 18.1 [8,9].

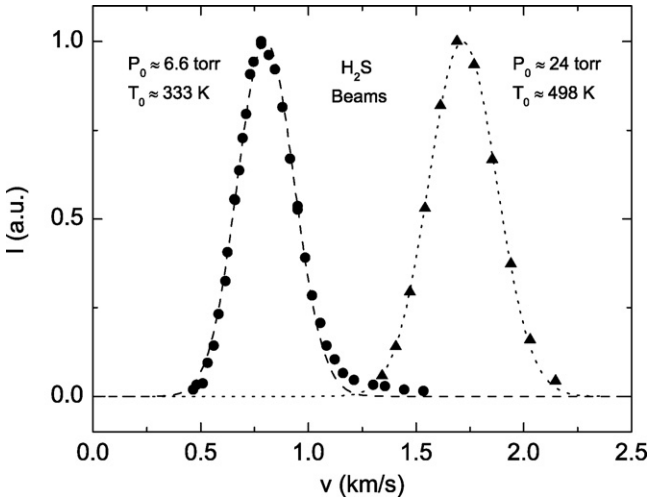

Fig. 5. Comparison between measured velocity distributions (circles and triangles) and calculations (dashed and dotted lines) using functions given in refs. [8,9], evaluated assuming a Mach number of 5.0 (left) and 8.7 (right), respectively.

The experimental points have been fitted according to the usual velocity distribution function of a supersonic molecular beam [8,9] at the source temperature of ~ 298 K (see inset in Fig. 4). The very good fitting of the data represents a robust test of the correct working of the new selector and at the same time it provides the calibration scale of the transmitted velocity v, since the supersonic Ar beam has a peak at 0.555 Km/s. Specifically, we have $v(\mathrm{Km/s}) = 0.0169(\pm 1\%) f(\mathrm{Hz})$, where f is the rotation frequency. Fig. 5 shows the measured velocity distributions for two molecular beams of H_2S generated under nearly effusive conditions (lower pressure) and under moderate supersonic conditions (higher pressure). Also shown are fits carried out with the procedure described above.

3. Scattering cross sections and information on the phenomenological spherical interaction

Fig. 6 reports $Q(v)$ data for the H_2S–He and H_2S–Xe systems, measured as a function of the selected velocity v of the H_2S projectile molecules. The results are plotted together with those for the H_2S–Ne, Ar and Kr systems, previously measured [1], in order to show the overall behavior of the complete H_2S–Rg family. Except for H_2S–He, in the probed velocity range the quantum mechanical glory effect is observed and appears as an oscillatory pattern $\Delta Q(v)$ overimposed to a smooth component, $\bar{Q}(v)$. The quantity $\bar{Q}(v)$ provides information about the long range attraction, while $\Delta Q(v)$ depends on the features of the potential well [10–12]. Again, except for the H_2S–He case, all cross section data are plotted as $Q(v)v^{2/5}$ to put into evidence the oscillatory structure associated to the glory interference.

As emphasized in the previous section, a heated source has been used and therefore the molecular beam contains rotationally hot H_2S molecules. In such conditions, it is reasonable to assume that during collisions with rare gases, the H_2S projectile molecules have sufficient time to smooth out the effect of the interaction anisotropy, making it possible to extract from $Q(v)$ information on an effective radial potential $V(r)$, namely the interaction averaged over all possible relative orientations [1,2]. Moreover, since the projectile molecules are rotationally hot and $Q(v)$ is mainly determined by collisional events at large and intermediate impact parameters, inelastic events can be assumed to play a minor role. Therefore, for the analysis of the experimental data it is suffi-

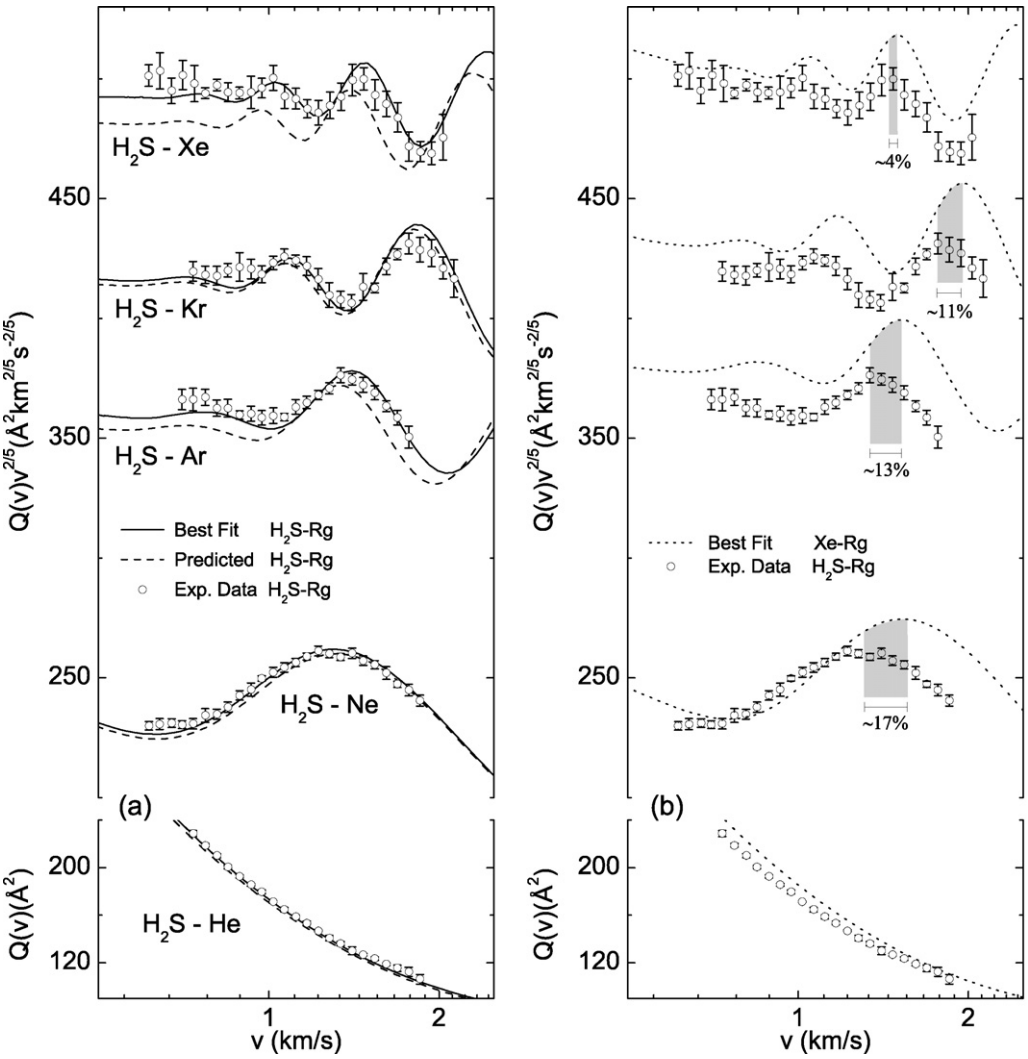

Fig. 6. Integral cross sections $Q(v)$, measured as a function of the selected molecular beam velocity v, for the H_2S–Rg family (circle symbols in (a) and (b)). In (a), calculations have been performed using the best fit (full lines) and predicted (dashed lines) parameters for H_2S–Rg. In (b), calculations have been performed using the best fit (dotted lines) parameters for the Xe–Rg family. These parameters are given in Table 1.

cient to take into account only the effect of elastic scattering [13].

For the analysis of $Q(v)$ data we adopted a recently proposed potential model [14], called Improved Lennard–Jones (ILJ). The ILJ model removes most of inadequacies, both at short and long range, of the familiar Lennard–Jones function. Moreover, it involves only a few parameters and therefore appears very useful for the analysis of experimental scattering data. According to the ILJ model, the functional form of the interaction potential is the following:

$$V(r) = \varepsilon \left[\frac{6}{n(r)-6} \left(\frac{r_m}{r} \right)^{n(r)} - \frac{n(r)}{n(r)-6} \left(\frac{r_m}{r} \right)^{6} \right], \quad (2)$$

where

$$n(r) = \beta + 4 \left(\frac{r}{r_m} \right)^2. \quad (3)$$

The ε parameter defines the potential well depth, r_m fixes the equilibrium distance and β is associated to the hardness of the involved chemical species, determining the shape of the potential in the region of the well. The β parameter is expected to be nearly constant for homologous systems. For the H_2S–Rg family we use $\beta = 9$, a value typical of van der Waals interactions [14]. Therefore, during the fitting procedure only ε and r_m have been varied. Since $\tilde{Q}(v)$ appears to be strongly affected by the r_m value, which depends on the second term in Eq. (2)[12], the absolute scale of $Q(v)$ has been adjusted within the experimental uncertainty (3–4%) of its calibration. In order to have a homogeneous pictures of the H_2S–Rg family, we have reanalyzed by the ILJ model also the data of the H_2S–Ne, Ar and Kr systems, for which we have given previously in ref. [1] a description in terms of a different functional form of the potential.

The cross sections $Q(v)$, calculated in the center of mass frame using the JWKB method combined with a fast and accurate semiclassical procedure [12], are convoluted in the laboratory system for the comparison with the experimental data. The convolution includes the average over the thermal motion of the target gas, the transmission function of the velocity selector, and a small correction to $Q(v)$ due to the finite angular resolution of the apparatus (the so called "limit angle" correction, due to the uncertainty principle) [4]. Such a correction, which depends on mass and velocity of the projectile, on the cross section value, and on the angular resolution of the experiment, is negligible for the scattering of H_2S by the lighter rare gases and becomes appreciable only for heavier Rg systems. Fig. 6(a) compares measured and calculated $Q(v)$, while Fig. 7 gives plots of the final

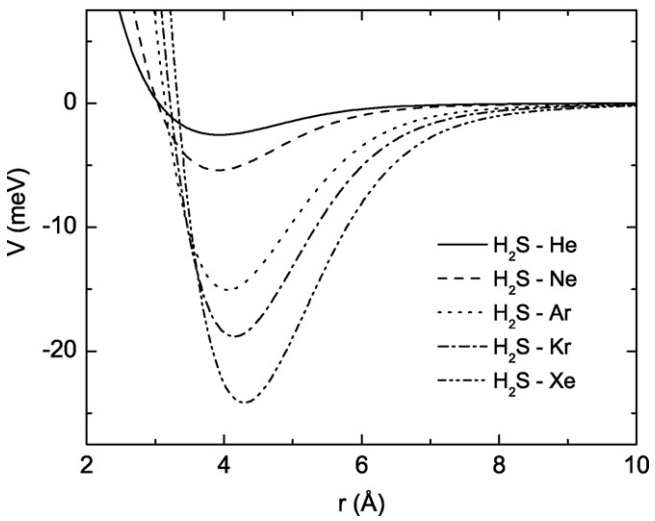

Fig. 7. Averaged interaction potential energy curves for H_2S systems obtained from the $Q(v)$ fit performed by using Eq. (2) and the parameters given in Table 1.

$V(r)$ for all systems. The corresponding parameters are reported in Table 1[17]. The same table also shows the values predicted by the correlation formulas [15,16], which provide ε and r_m for a typical V_{vdW} interaction, including the slight perturbation by induction effects. In particular, such formulas have been applied by taking into account the polarizabilities of H_2S and rare gases, and including the effect due to the permanent dipole of H_2S [1].

Cross sections calculated using these parameters are plotted in Fig. 6 as dashed lines. The comparisons reported both in Table 1 and in Fig. 6 clearly demonstrate that the interaction in H_2S–Rg is basically of van der Waals nature. However, for H_2S–Xe, the small shift in the glory extrema position [2](see Fig. 6), between $Q(v)$ calculated using the best fit potential and that predicted by the correlation formulas suggests that, for this system, an additional attractive component is operative. Such component originates an appreciable increase (by 5–10%) of the potential well depth (see also the comparison between the ε values in Table 1).

A complementary way to unravel the nature of interaction in the H_2S–Rg family, and to better quantify possible small effects due to interaction components additional to the van der Waals, is based on the comparison with calculations of $Q(v)$ using the potential parameters of the Xe–Rg systems. The complete family of Rg–Rg systems has been recently the target of a multiproperty analysis [18], using the potential model of Eq. (2) in order to test its effectiveness in a wide r range. The parameters for Xe–Rg (reported in Table 1) are directly used in the present analysis and the so calculated $Q(v)$ are reported as dotted line in Fig. 6(b). This comparison is motivated by the closeness of the polarizability values of H_2S ($\alpha = 3.78$ Å^3) [1] and Xe ($\alpha = 4.04$ Å^3) [15]. In particular, correlation formulas [15] suggest that if the interactions in all H_2S–Rg systems are of van der Walls nature, they should exhibit a potential well deeper by ~ 15–20% with respect to the corresponding H_2S–Rg and this effect should originate a shift of the same amount in the glory extrema position between measured and calculated $Q(v)$. This expected behavior is well evident for the Ne case (see Fig. 6(b)) and tends to attenuate when the heavier Rg atoms are considered. This confirms that the H_2S–Xe system, for which the well depth tends to be nearly coincident with that of the Xe–Xe system, represents the case where the additional component characterized above emerges in a more evident way. As a comparison, we note that for the case of water–rare gas complexes we discovered similar but much larger effects [2]. They could already be clearly seen for H_2O–Ar and present the largest value (~ 30%) for the H_2O–Xe system.

In conclusion, the study of the strength, nature and role of such an additional component, appearing in a more pronounced way in homologous cases involving water, is of particular interest for the investigation of the hydrogen bond formation. Experimental investigations on systems involving both H_2S and H_2O interacting with molecular partners are in progress. Theoretical research has been reported on the H_2O_2–Rg systems [19]. The relevance of these studies for atmospheric science has been recently reviewed [20].

Table 1
Well depth ε and equilibrium distance r_m obtained by the best fit of $Q(v)$ with ILJ model and comparison with values predicted by correlations formulas [15,16]

System	Best fit		Predicted	
	ε (meV)	r_m (Å)	ε (meV)	r_m (Å)
H_2S–Xe	24.14	4.290	22.86	4.286
Xe–Xe	24.20	4.350		
H_2S–Kr	18.80	4.150	18.53	4.150
Xe–Kr	19.95	4.200		
H_2S–Ar	15.05	4.050	14.31	4.057
Xe–Ar	16.09	4.100		
H_2S–Ne	5.40	3.910	5.48	3.889
Xe–Ne	6.35	3.885		
H_2S–He	2.55	3.932	2.62	3.878
Xe–He	2.62	3.995		

The corresponding ones for the Xe–Rg systems are also reported. 1 meV = 0.096485 kJ mol^{-1}; 1 Å = 0.1 nm.

Acknowledgements

This paper is our contribution in honor of Zdenek Herman, a pioneer and guide for many of us in the adventurous territory of ion molecule reactions. The work has been supported by the Italian Ministero dell' Universita e Ricerca (MIUR) and by Italian Agenzia Spaziale (ASI). We thank Giovanni and Andrea Nicoziani for technical assistance. L.F. Roncaratti acknowledges the Alban Programme scholarship of the European Union.

References

[1] D. Cappelletti, A.F.A. Vilela, P.R.P. Barreto, R. Gargano, F. Pirani, V. Aquilanti, J. Chem. Phys. 125 (2006) 133111.
[2] V. Aquilanti, E. Cornicchi, M.M. Teixidor, N. Saending, F. Pirani, D. Cappelletti, Angew. Chem. Int. Ed. 44 (2005) 2356.
[3] D. Cappelletti, V. Aquilanti, E. Cornicchi, M.M. Teixidor, F. Pirani, J. Chem. Phys. 106 (2005) 024302.
[4] D. Cappelletti, M. Bartolomei, F. Pirani, V. Aquilanti, J. Phys. Chem. A 106 (2002) 10764.
[5] T. Nenner, H. Tien, J.B. Fenn, J. Chem. Phys. 63 (1975) 5439.
[6] F. Pirani, F. Vecchiocattivi, J. Chem. Phys. 66 (1977) 372.
[7] F. Pirani, D. Cappelletti, F. Vecchiocattivi, L. Vattuone, A. Gerbi, M. Rocca, U. Valbusa, Rev. Sci. Instrum. 75 (2004) 349.
[8] J.B. Anderson, R.P. Andres, J.B. Fenn, Adv. Chem. Phys. 10 (1966) 275.
[9] G. Scoles (Ed.), Atomic and Molecular Beam Methods, Oxford University Press, New York, Oxford, 1988.
[10] R.B. Bernstein, T.J. O'Brien, Discuss, Faraday Soc. 40 (1965) 35.
[11] R.B. Bernstein, R.A. La Budde, J. Chem. Phys. 58 (1973) 1109.
[12] F. Pirani, F. Vecchiocattivi, Mol. Phys. 45 (1982) 1003.
[13] V. Aquilanti, D. Ascenzi, D. Cappelletti, M. de Castro, F. Pirani, J. Chem. Phys. 109 (1998) 3889.
[14] F. Pirani, M. Alberti, A. Castro, M. Moix Teixidor, D. Cappelletti, Chem. Phys. Lett. 394 (2004) 37.
[15] R. Cambi, D. Cappelletti, F. Pirani, G. Liuti, J. Chem. Phys. 95 (1991) 19852.
[16] F. Pirani, G. Maciel, D. Cappelletti, V. Aquilanti, Int. Rev. Phys. Chem. 25 (2006) 165.
[17] Although the present analysis has been carried out with a different potential model, the ε and r_m parameters here obtained for the H_2S–Ne, Ar and Kr systems

are the same as those presented in ref. [1]. Note that the C_6 values in Table 1 of ref. [1] should be in units of 10^{-4} kJ mol^{-1} nm^6.
[18] F. Pirani, S. Brizi, L.F. Roncaratti, P. Casavecchia, D. Cappelletti, F. Vecchiocattivi, Phys. Chem. Chem. Phys., 10 (2008), doi:10.1039/b808524b.
[19] P.R.P. Barreto, A.F.A. Vilela, A. Lombardi, G.S. Maciel, F. Palazzetti, V. Aquilanti, J. Phys. Chem. A 111 (2007) 12754.
[20] G.S. Maciel, D. Cappelletti, G. Grossi, F. Pirani, V. Aquilanti, Adv. Quant. Chem. 55 (2008) 311.